Nanoscale

Accepted Manuscript

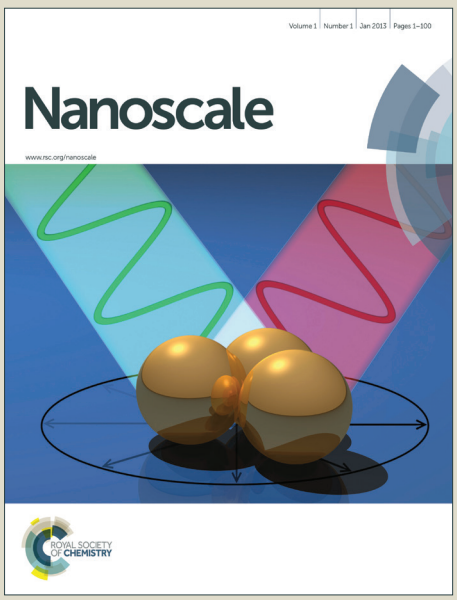

ROYAL SOCIETY OF CHEMISTRY

www.rsc.org/nanoscale

Journal Name

RSCPublishing

ARTICLE

Bipyridine hydrogel for selective and visible detection and absorption of Cd^{2+}

Cite this: DOI: 10.1039/x0xx00000x

Qingqing Miao,[a] Ziye Wu,[c] Zijuan Hai,[a] Changlu Tao,[d] Qingpan Yuan,[a] Yadi Gong,[a] Yafeng Guan,[b] Jun Jiang,*[c] and Gaolin Liang*[a]

Received 00th January 2012,
Accepted 00th January 2012

DOI: 10.1039/x0xx00000x

www.rsc.org/

Herein, we report for the first time using bipyridine-based hydrogel for selective and visible detection and absorption of Cd^{2+}. At low concentrations, hydrogelator **1** was applied for selective detection of Cd^{2+} in vitro and in living cells with high sensitivity. In the absence of metal ions, **1** is nonfluorescent at 470 nm. Upon addition of metal ions, **1** selectively coordinates with Cd^{2+}, causing 86-fold increase of fluorescence intensity at 470 nm via chelation enhanced fluorescence (CHEF) effect, as revealed by first-principles simulations. At 1.5 wt% and pH 5.5, **1** self-assembles into nanofibers to form hydrogel **Gel I**. Since Cd^{2+} could actively participate in the hydrogelation and promote the self-assembly, we also successfully applied **Gel I** for visible detection and absorption of Cd^{2+}. With these excellent properties, **Gel I** is expected to be explored as one type of versatile biomaterials for not only environmental monitoring but also pollution treatment in the near future.

Introduction

Cadmium is one of the important metals and widely used in many fields such as electroplating, metallurgy, agriculture, military affairs, etc.[1] However, cadmium is extremely toxic and carcinogenic, listed by the U.S. Environmental Protection Agency (EPA) as one of 126 priority pollutants. It can accumulate in the human body for more than 10 years, consequently resulting in increased risks of cardiovascular diseases, cancer mortality, and damage to liver and kidneys.[2] Thus, there is an increasing need for developing new methodologies for quick and specific detection of cadmium ions in vitro and in vivo, as well as for its absorption.

To date, a number of instrument-based technologies have been developed for the detection of cadmium ions including atomic absorption spectrometry (AAS),[3-5] atomic fluorescence spectrometry (AFS),[6, 7] colorimetry,[8, 9] inductively coupled plasma atomic emission spectroscopy (ICP-AES),[10] inductively coupled plasma mass spectrometry (ICP-MS),[11] X-ray fluorescence,[12] electrochemistry,[13] surface enhanced Raman scattering (SERS).[14] The limits of detection (LODs) of these technologies are within the wide range of 10^{-4}-10^{-9} M, except those of ICP-MS and AAS are at 10^{-11} M level (Table S3†). But fluorometry has its own advantages over these techniques in operational simplicity and high sensitivity.[15-17] So far, many types of fluorescent sensors, including small molecule-based chemosensors,[1, 15, 18] calixarene-based chemosensors,[19] protein-[20] or functional materials-based sensing systems,[21-25] have been developed for the detection of cadmium ions. Nevertheless, before being applied for detection of cadmium ions in biological samples, fluorescent sensors need to overcome their intrinsic weaknesses such as unsuited pH range,[26] tedious procedures of sample preparation,[27] poor biocompatibility,[28] or poor selectivity[29].

Supramolecular hydrogels are composed of small amount (normally less than 5%) of three-dimensional (3D) networks (e.g., nanofibers) gelling large amount (more than 95%) of water.[30-32] Due to their inherent good properties (e.g., biocompatibility and biodegradability) as biomaterials, hydrogels have attracted broad research interests and been extensively explored in recent years.[33-35] In addition to their wide applications in tissue engineering and enzyme immobilization,[36, 37] hydrogels have recently shown very exciting and promising applications for sensing metal ions or detection of biomarkers.[38, 39] Moreover, hydrogels also have been reported for the absorption of hazardous heavy metal ions such as uranium.[40, 41] However, to the best of our knowledge, there is no supramolecular hydrogel reported for either the detection or the absorption of Cd^{2+}. Current strategies for cadmium absorption include chemical precipitation, ion exchange and adsorption, etc.[42]

Inspired by these pioneering studies mentioned above, we aimed to design hydrogelators for quick and selective detection of Cd^{2+} in physiological conditions (e.g., buffers at pH around 7.4) and use their hydrogels to remove this hazardous metal ion. Meanwhile, we intend to visibly trace the processes of detection and absorption. Thus, as shown in Fig. 1, we rationally designed bipyridine-derivatived hydrogelator **1** for these purposes because a lot of pyridine derivatives have been reported to have strong fluorescence upon the additions of metal ions.[1, 29, 43] We found that **1** can

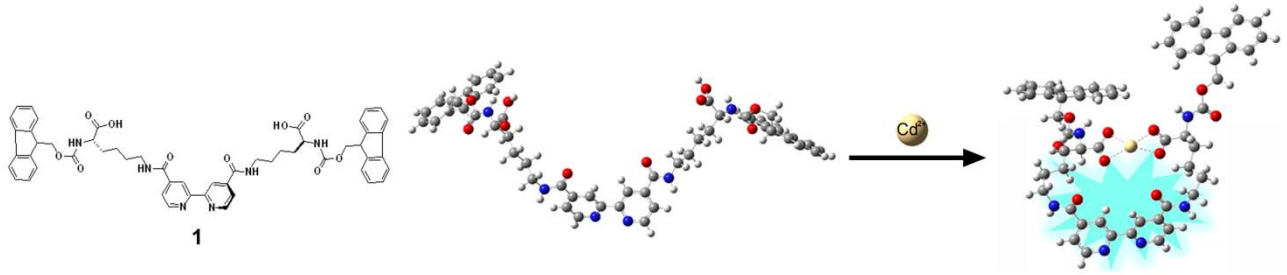

Fig. 1 Schematic illustration of fluorescence "turn on" of **1** for selective detection of Cd^{2+}.

selectively and specifically coordinate with Cd^{2+}, turning on its fluorescence emission at 470 nm (86-fold increase). Interestingly, 1.5 wt% of this bipyridine derivative **1** in water at pH 5.5 self-assembles into nanofibers to form hydrogel and the hydrogel was successfully applied to visibly detect and absorb Cd^{2+}.

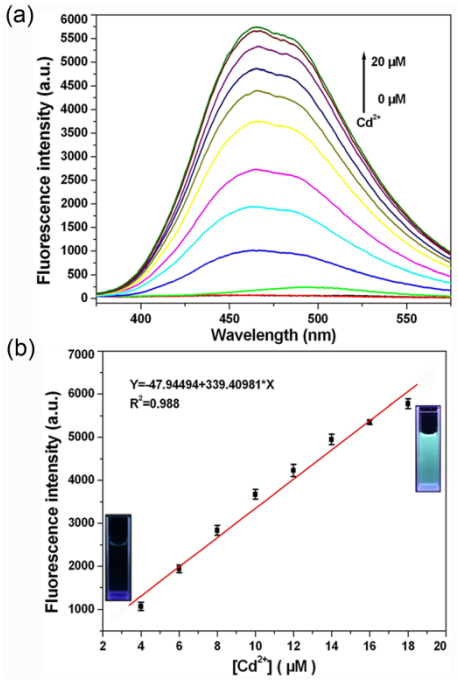

Fig. 2 (a) Fluorescence spectra of **1** (20 μM, λ_{ex} = 300 nm) in the presence of various concentrations of Cd^{2+} (0, 1, 2, 4, 6, 8, 10, 12, 14, 16, 18, or 20 μM) in phosphate buffer (10 mM, pH 7.5) containing 10% ethanol at room temperature. (b) Fitted calibration curve of the fluorescence intensity at 470 nm in Fig. a as a function of Cd^{2+} concentrations. The inset fluorescent photographs show the fluorescence changes of **1** at 20 μM before and after addition of 20 μM Cd^{2+} under a UV lamp.

Results and discussion

Syntheses and rationale of the design

We began the study with the syntheses of the precursor 4,4'-dicarboxysuccinimidyl-2,2'-bipyridine and probe **1**. The syntheses are facile and straightforward as follows, which are according to literature method[44] (Scheme S1): 4,4'-dicarboxysuccinimidyl-2,2'-bipyridine was synthesized by activating 2,2'-bipyridinyl-4,4'-dicarboxylic acid with N- hydroxy-succinimide and dicyclohexylcarbodiimide and then purified by recrystallization. 4,4'-dicarboxysuccinimidyl-2,2'-bipyridine was then coupled with Fmoc-Lys-OH-HCl, purified with HPLC to yield **1**. **1** was designed to have two components as following: (1) a bipyridine group for providing fluorophore to turn on the fluorescence after Cd^{2+} coordination, and (2) two symmetric amphiphilic Fmoc-Lys-OH parts for self-assembling to form hydrogel and coordination with Cd^{2+}. Using **1**, we were able to specifically detect Cd^{2+} in water and in cells, and visibly absorb Cd^{2+} at high concentration (i.e., with **Gel I**).

Detection of Cd^{2+} in vitro

Fig. 2a shows the fluorescence spectra of **1** at 20 μM (λ_{ex} = 300 nm) in the presence of various concentrations of Cd^{2+} (0 to 20 μM). With increasing concentrations of Cd^{2+}, the spectra clearly showed a gradual increase of emission intensity at 470 nm and reached 86 folds eventually. Interestingly, further addition of Cd^{2+} would not induce the increase of fluorescence emission any more, echoing that **1** chelates Cd^{2+} with an 1:1 stoichiometry (Fig. S5†). Corresponding UV-vis absorption spectra of **1** showed the appearance of a new peak at 330 nm upon Cd^{2+} addition, suggesting the formation of the **1**-Cd^{2+} complex (Fig. S6†). In contrast, neither UV-vis spectra nor fluorescence spectra of 2,2'-bipyridinyl-4,4'-dicarboxylic acid showed obvious change upon the addition of Cd^{2+} (Fig. S7†), indicating that it is the Fmoc-Lys-OH motifs on **1** that coordinate with Cd^{2+} to turn the fluorescence on. Additionally, we also conducted ^{1}H NMR study to confirm the chelation between **1** and Cd^{2+}. ^{1}H NMR spectra of **1** showed that the proton resonances on the bipyridine rings were shifted downfield and became broader upon addition of one equiv. of Cd^{2+} (Fig. S8†). The downfield shifts and broadenings of proton resonances were respectively induced by restricted rotation of pyridine rings and nonbonding H-H repulsions among the pyridine rings, both of which are all required for Cd^{2+} complexation and therefore indicate the coordination of Cd^{2+} to **1**. A Job's plot indicated that **1** indeed chelates Cd^{2+} with an 1:1 stoichiometry (Fig. S9†). Using Fig. 2a, we

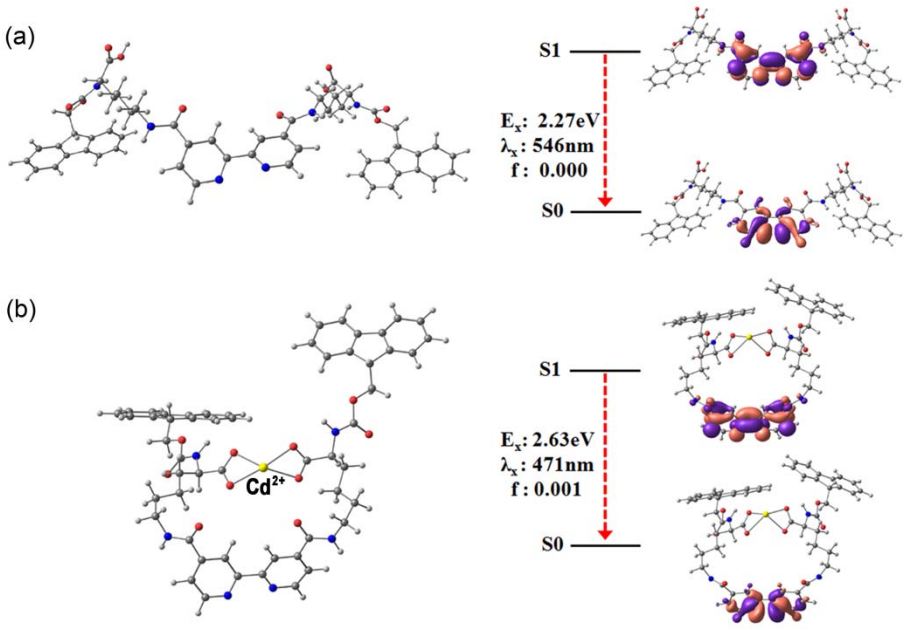

Fig. 3 The optimized molecular structures together with the transition orbital energies and wavefunctions of the lowest excited state of the compound **1** (a) and **1**-Cd^{2+} (b), respectively.

calculated the binding constant K for the coordination between **1** and Cd^{2+} at pH 7.5 to be $1.1 \times 10^5\ M^{-1}$,[45] slightly higher than that between bipyridine and Cd^{2+} (log K = 4.2).[43] At pH 6.0 and 9.0, **1** has binding constants of $1.8 \times 10^5\ M^{-1}$ and $9.7 \times 10^4\ M^{-1}$ to Cd^{2+}, respectively (Fig. S10†), suggesting that acidic environment benefits the binding of Cd^{2+} to **1**. By correlating the value of the fluorescence intensity at 470 nm with the concentration of Cd^{2+}, we constructed a calibration curve for the determination Cd^{2+} in water. As shown in Fig. 2b, a linear relationship between the value of the fluorescence intensity at 470 nm and Cd^{2+} concentration ($Y = 47.94494 + 339.4.981X$, $R^2 = 0.988$) was obtained over the range of 4 – 18 μM. The limit of detection (LOD) of Cd^{2+} in this assay was 21 nM ($S/N = 3$) which is one order of magnitude lower than those of previously reported fluorescence probes for Cd^{2+} detection (Table S3†). These indicated that **1** is an excellent chelation enhanced fluorescence (CHEF) sensor for Cd^{2+} detection with high sensitivity.

Mechanisms of fluorescence induction

We then carried out theoretical investigations to examine the different addition effects of Cd^{2+} ions to **1** and its precursor. We have firstly reproduced the experimentally measured absorbance spectrum of the precursor 4,4'-dicarboxysuccinimidyl-2,2'-bipyridine, which validated the theoretically optimized molecular structure (Fig. S7†). Based on the precursor, the molecular structure of **1** was built and optimized as in Fig. 3a. As shown in Fig. 3b, the computed structure of a Cd^{2+} ion adding to **1** revealed that Cd^{2+} tends to bond with four oxygen atoms of two -COOH groups in **1**, in which two protons were deprotonated at pH 7.5 for Cd^{2+} detection. It is clear that the Cd^{2+} addition has converted the linear molecule of **1** into a circle, naturally changing the conjugation of the molecule as well as its electron distributions. As a result, the measured absorbance spectra of **1**-Cd^{2+} complexes exhibit an increasing absorption peak at ~311 nm with the increase of Cd^{2+} concentration (Fig. S6a†), which was well explained by the computed electronic transitions involving the **1**-Cd^{2+} bondings (Fig. S6b†).

Consequently, the transition from the first excited state of **1** to its ground state has been greatly altered by the formation of **1**-Cd^{2+} bonds, with transition ability increasing from zero to 0.001 as shown in Fig. 3. The predicted photoluminescence peak is blueshifted from 546 nm to 471 nm, agreeing well with experimental spectra. These demonstrate that coordination of **1** with Cd^{2+} ions induces the conformation change of **1**, resulting in the enhancement and blueshift of the its fluorescence.

Selectivity, specificity, and recovery of 1 for Cd^{2+} detection

Selectivity is one of the important parameters to evaluate the performance of a new fluorescence probe. Particularly, for a cellular imaging probe which potentially has biomedical or environmental applications, a highly selective response to the target over other potentially competing species is a necessity. Therefore, the selectivity study of **1** to Cd^{2+} over various metal ions such as abundant cellular cations (e.g., Ca^{2+} and Mg^{2+}), essential metal ions in cells (e.g., Co^{2+}, Fe^{3+}, Zn^{2+}, Fe^{2+}, Ni^{2+}, Sr^{2+}, Ba^{2+}), and environmentally relevant heavy metal ions (e.g., Hg^{2+}, Ag^{+}, Pb^{2+},Cr^{3+},Cu^{2+}), was conducted. As shown in Fig. 4a, among these metal ions tested, only Cd^{2+} selectively responds to **1** except Zn^{2+} has an extremely weak response. The fluorescent photographs of **1** in a cuvette in the presence of different metals (20 μM) under a UV

lamp, corresponding to Fig. 4a, were shown in Fig. 4c. Fluorescence responses of 20 μM **1** to 20 μM Cd^{2+} in the presence of other metal ions (20 μM) were also measured (Fig. 4b), and the results indicated that the detection of Cd^{2+} was not influenced by most of the metal ions tested (Sr^{2+}, Hg^{2+}, Mg^{2+}, Ag^{+}, Pb^{2+}, Ca^{2+}, Ba^{2+}, Fe^{3+}). In the presence of metal ions (M^{n+}) Fe^{2+}, Zn^{2+}, Cr^{3+}, Cu^{2+}, Co^{2+}, or Ni^{2+}, which theoretically are able to chelate with bipyridine motifs, coordination between **1** and Cd^{2+} seemed to be slightly interfered by these metal ions by decreasing the ratios of fluorescence intensity of **1**-Cd^{2+} + M^{n+}/**1** + M^{n+} (the lowest ratio is 6.6 for Zn^{2+}, the original ratio for **1**-Cd^{2+}/**1** is 85.9). These results indicate that **1** also has good specificity toward Cd^{2+}. With the purpose of illustrating the reliability and accuracy of the assay proposed, we also used pond water as a real sample for Cd^{2+} detection with **1**. As shown in Table S2 (†), the mean recovery for each sample was within the range of 96% to 97%, suggesting that this assay is applicable for Cd^{2+} detection in real-world samples. In brief, probe **1** has excellent selectivity and good specificity to Cd^{2+} over most competing metal ions and can be applied for Cd^{2+} detection in real samples.

Theoretical investigations have also been performed on the systems of **1**-Zn^{2+} and **1**-Ag^{+}. As expected, the Zn^{2+} ions can form effective bondings with four oxygen atoms in the complex (Fig. S11a†), while Ag^{+} only weakly bonds to two oxygen atoms of **1** (Fig. S11b†). These well explain the results of selectivity study (i.e., enhancement of fluorescence) of **1** over different metal ions in Fig. 4a.

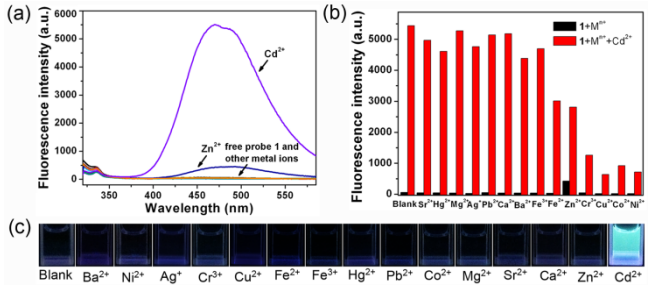

Fig. 4 (a) The fluorescence spectra of **1** (20 μM, λ_{ex} = 300 nm) in the presence of different metal ions (20 μM) in phosphate buffer (10 mM, pH 7.5) containing 10% ethanol at room temperature (RT). (b) Fluorescence responses of **1** (20 μM) toward Cd^{2+} (20 μM) in the presence of one equiv. of different metal ions in phosphate buffer (10 mM, pH 7.5) containing 10% ethanol at RT. (c) The corresponding fluorescent photographs of **1** (20 μM) in a cuvette in the presence of different metals (20 μM) under a UV lamp.

Sensing Cd^{2+} in living cells

After the above studies, we further investigated the applicability of **1** for the detection of Cd^{2+} in living cells. Before that, we studied the cytotoxicity of **1**. 3-(4,5-dimethylthiazol-2-yl) 2,5 diphenyltetrazolium bromide (MTT) assay indicated, after being incubated with **1** at 20 μM, 40 μM, or 80 μM for one day, 113%, 111%, or 80% of the HepG2 cells survived respectively (Fig. S12a†), suggesting **1** is safe for HepG2 cell imaging. When the cells were incubated with 20 μM, 40 μM, or 80 μM **1** for three days, 118%, 97% or 83% of the cells survived respectively, suggesting **1** is not toxic to the cells until three days (Fig. S12a†). Similarly, MTT assay indicated, after being incubated with **1** at 20 μM, 40 μM, or 80 μM for one day, 110%, 100%, or 76% of the human colon carcinoma LoVo cells survived respectively (Fig. S12b†), suggesting **1** is safe for LoVo cell imaging. When the cells were incubated with 20 μM, 40 μM, or 80 μM **1** for two days, 109%, 105% or 80% of the cells survived respectively, suggesting **1** is not toxic to the cells until two days (Fig. S12b†). As shown in Fig. 5, without addition of Cd^{2+}, HepG2 cells treated with 20 μM **1** showed very weak fluorescence. With the increase of the concentration of Cd^{2+} added, fluorescence emission from cells that subsequently treated with 20 μM **1** increased which suggests that **1** not only could penetrate the cell membrane but also has a selective response to Cd^{2+} over other intracellular metal ions (e.g., Na^{+}, K^{+}, Ca^{2+}, Mg^{2+}, etc.) or biomolecules. Moreover, healthy cell morphology also suggested that **1** was biocompatible to HepG2 cells at this concentration. The average fluorescence intensity of the HepG2 cells in Fig. 5 was measured with Image J and summarized in Fig. S14a†. The results indicated that fluorescence intensities of cells incubated with 5, 10, or 20 μM Cd^{2+} are 1.57, 2.02 or 3.30 folds of that of control cells (i.e., 0 μM Cd^{2+} followed by 20 μM **1** treatment), respectively (Fig. S14a†). Futhermore, we also applied **1** for the detection of Cd^{2+} in LoVo cells (Fig. S13†). The results indicated that fluorescence intensities of cells incubated with 5, 10, or 20 μM Cd^{2+} are 1.32, 2.29, or 3.94 folds of that of control cells (i.e., 0 μM Cd^{2+} followed by 20 μM **1** treatment), respectively (Fig. S14b†). All these results suggest that **1** could be used to image intracellular Cd^{2+} in living cells and therefore be potentially applied for the study of toxicity or bioactivity of Cd^{2+} in living cells.

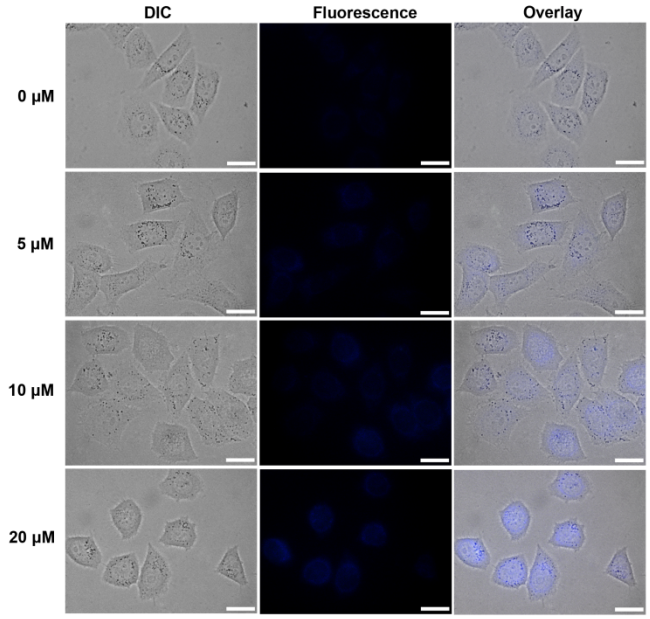

Fig. 5 Differential interference contrast (DIC) images (left), fluorescence images (middle, DAPI channel), and merged images (right) of HepG2 cells incubated with 0, 5, 10, or 20 μM of Cd^{2+} in serum-free medium for 0.5 h at 37 °C, washed with PBS for three times, then incubated with 20 μM **1** in serum-free medium for 0.5 h at 37 °C prior to imaging, respectively. Scale bar: 20 μm.

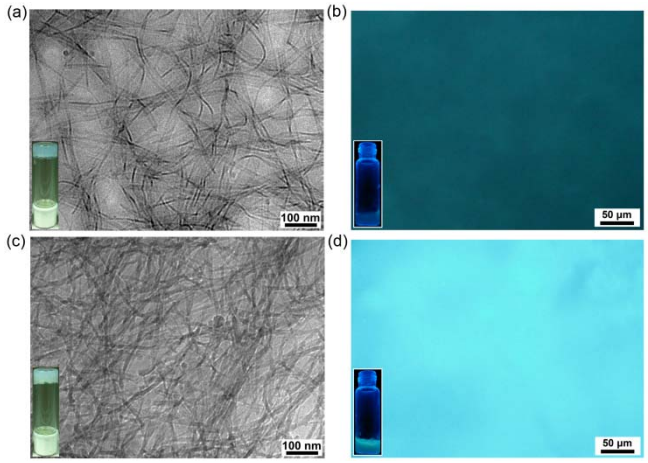

Fig. 6 (a, c) cryo-TEM images of **Gel I** (a) and **Gel I** + Cd^{2+} (c), respectively. The insets are white light photographs of **Gel I** and **Gel I** + Cd^{2+} at 1.5 wt% and pH 5.5, respectively. (b, d) Fluorescence images (DAPI channel) of **Gel I** (b) and **Gel I** + Cd^{2+} (d) on glass slides, respectively. The insets are fluorescent photographs of **Gel I** and **Gel I** + Cd^{2+} in vials under a 365 nm UV lamp, respectively.

Gelation of 1 and visible detection of Cd^{2+} with Gel I

By pH adjustment, water solutions of **1** were able to form supramolecular hydrogels in the presence (the inset in Fig. 6c) or absence of Cd^{2+} (the inset in Fig. 6a). In brief, 7 mg of **1** was suspended in 400 μL of water. Adjustment of the pH values of above suspension to 8.5 with 1 M NaOH resulted in clear solution. Carefully adjusting the pH values of above solution to 5.5 with 0.1 M HCl afforded opaque **Gel I** (the inset in Fig. 6a). The aggregation process of **1** at pH 5.5 was further studied with UV−vis spectroscopy (Fig. S15†). Plots of optical transmittance at 425 nm of **1** versus its concentration revealed two regimes, which indicate the critical aggregation concentration (CAC) of 16 μM for **1** at pH 5.5.[46] As for the preparation of **Gel I** + Cd^{2+}, Cd^{2+} (one equiv. to **1**) was added into the turbid solution of **1** at pH around 6, then the pH value of the mixture was adjusted to 5.5 to afford opaque hydrogel (the inset in Fig. 6c). The microscopic structure of **Gel I** under cryo-TEM exhibited regularly arranged, long fibers with an average width of 7.6 ± 1.2 nm (Fig. 6a). Interestingly, the fibers tend to bundle together to form thicker fibers with an average width of 27.1 ± 6.8 nm (Fig. 6a). Cryo-TEM image of **Gel I** + Cd^{2+} showed more entangled, denser, longer, and slimmer nanofibers than those of Gel **I**, with an average width of 12.6 ± 3.4 nm (Fig. 6c). These results suggest that Cd^{2+} successfully chelate with gelator **1**, consequently affecting the self-assembling modes and promoting the gelation ability of **1**. Energy-dispersive X-ray spectroscopic (EDS) elemental analysis of Gel **I** + Cd^{2+} proved the existence of Cd in the nanofibers (Fig. S16†), suggesting Cd^{2+} indeed coordinates with **1** to form a stable **1**-Cd^{2+} complex. When the hydrogels were under a UV illumination at 365 nm, **Gel I** exhibited weak purplish blue fluorescence (the inset in Fig. 6b) while **Gel I** + Cd^{2+} showed strong azure fluorescence (the inset in Fig. 6d). Using a fluorescence microscopy to image **Gel I** (Fig. 6b) and Gel **I** + Cd^{2+} (Fig. 6d), we were able to quantitate their fluorescence emission in DAPI channel with Image J. The results indicate that the fluorescent intensity of **Gel I** + Cd^{2+} is 3.13 folds of that of **Gel I** (Fig. S17†), suggesting **Gel I** could be utilized for rapid and visible detection of Cd^{2+}.

Visible absorption of Cd^{2+} with Gel I

Since we have demonstrated that Cd^{2+} can actively participate in the hydrogelation of **1** and thereafter turn the fluorescence of **Gel I** on, we decided to use **Gel I** for visible detection and absorption of Cd^{2+} simultanously. As shown in Fig. 7, under a 365 nm UV lamp, 1 mg $CdCl_2$ powder is totally nonfluorescent and 300 μL **Gel I** emits very weak purplish blue fluorescence. Once they were fully mixed, 1 mg $CdCl_2$ powder was totally absorbed by 300 μL **Gel I** and very strong azure fluorescence was observed from the mixture. With this excellent property of visible detection and absorption of Cd^{2+}, **Gel I** is expected to be a versatile biomaterial applicable for not only environmental monitoring but also pollution treatment in the future.

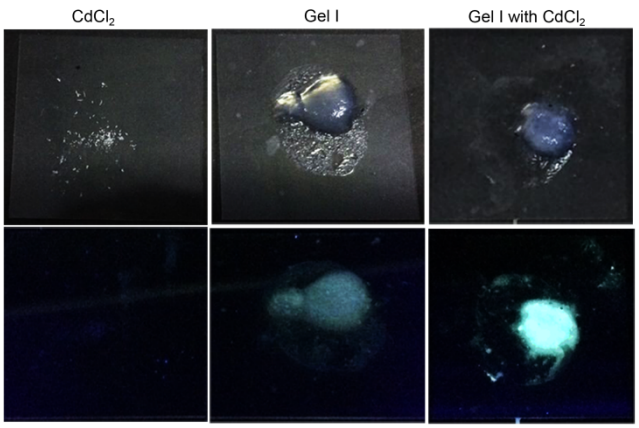

Fig. 7 Upper: white light photographsof 1 mg $CdCl_2$ powder, 300 μL **Gel I**, and 300 μL **Gel I** mixed with 1 mg $CdCl_2$, respectively. Lower: corresponding fluorescence photographs of 1 mg $CdCl_2$ powder, 300 μL **Gel I**, and 300 μL **Gel I** mixed with $CdCl_2$ under a 365 nm UV lamp, respectively.

Conclusions

In conclusion, we have successfully developed a bipyridine-based hydrogelator **1** for specific detection of Cd^{2+} in vitro and in living cells with high sensitivity. Upon chelation with 20 μM Cd^{2+}, fluorescence emission of 20 μM **1** at 470 nm was significantly enhanced about 86 folds. This property was successfully applied for highly selective detection of Cd^{2+} within the range of 4-18 μM and a LOD of 21 nM. Interference study proved that **1** was specifically responsive to Cd^{2+}. Theoretical simulations revealed the underlying mechanism that satisfactorily explained experimental results of such fluorescence turn-on of **1** upon Cd^{2+} chelation with high selectivity. Cell imaging study indicated that **1** is biocompatible and cell permeable, and could be applied to image Cd^{2+} in living cells. Since Cd^{2+} actively participates in the hydrogelation process of **1** and promotes the self-assembly, we also successfully applied **Gel I** for visible detection and absorption of Cd^{2+}. With these excellent properties, **Gel I** is expected to be explored as one type of versatile biomaterials for not only environmental monitoring but also pollution treatment in the near future.

Experimental

Materials

All the starting materials were obtained from Sigma or Sangon Biotech. Commercially available reagents were used without further purification, unless noted otherwise. All chemicals were reagent grade or better.

General methods

^{1}H NMR and ^{13}C NMR spectra were obtained on a Bruker AV 300. Matrix-assisted laser desorption (MALDI) ionization-time of flight (TOF)/TOF and ESI mass spectra were obtained on a time-of-flight Ultrflex II mass spectrometer (Bruker Daltonics) and on a Finnigan LCQ Advantage ion trap mass spectrometer (ThermoFisher Corporation) equipped with a standard ESI source, respectively. High performance liquid chromatography (HPLC) purification was performed on a Shimazu UFLC system equipped with two LC-20AP pumps and an SPD-20A UV/vis detector using a Shimazu PRC-ODS column. HPLC analyses were performed on an Agilent 1200 system equipped with a G1322A pump and in-line diode array UV detector an Agilent Zorbax 300SD-C18 RP column, with CH_3CN (0.1% of TFA) and water (0.1% of TFA) as the eluent. Cell images were obtained on the IX71 fluorescence microscope (Olympus, Japan). Cryo transmission electron micrographs (cryo-TEM) were obtained on a Tecnai F20 Transmission Electron Microscope from FEI company, operating at 200 kV. The cryo-samples were prepared as following: a special copper grid coated with carbon was put into Gatan SOLARUSTM plasma-cleaning system to remove hydrocarbon contamination on the sample holder, and then the sample was dropped on the copper grid in FEI Vitrobot sample plunger. The sample preparation was completed in the plunger. UV-vis absorbance spectra were recorded on a lambda 25 UV-visible spectrophotometer (PerkinElmer, America) at room temperature. Fluorescence spectra were recorded on a F-4600 fluorescence spectrophotometer (Hitachi High-Techonologies Corporation, Japan) with excitation wavelength set to 300 nm.

Synthesis and characterization of 4,4'-dicarboxysuccinimidyl-2,2'-bipyridine

2,2'-Bipyridinyl-4,4'-dicarboxylic acid (1.00 g, 4.1 mmol) and N-hydroxysuccinimide (0.95 g, 8.2 mmol) were dissolved in 40 mL dry DMF. Then dicyclohexylcarbodiimide (1.70 g, 8.2 mmol) dissolved in 10 mL DMF was added. The mixture was stirred for 12 h and then filtered to remove the dicyclohexylurea. Solvent of the filtrate was removed under vacuum, and the resulting solid was recrystallized with dichloromethane to yield the 4,4'-dicarboxysuccinimidyl-2,2'-bipyridine (1.10 g; 2.5 mmol, 61 %). ^{1}H NMR (300 MHz, d_6-DMSO, Fig. S1†) δ (ppm): 9.10 (d, J = 5.1 Hz, 2 H), 8.93 (s, 2 H), 8.14 (d, J= 5.7 Hz, 2 H), 2.94 (s, 8 H).

Synthesis and characterization of 1

Fmoc-Lys-OH-HCl (1.104 g, 2.5 mmol) was dissolved in 15 mL dry DMF and then DIEA (400 µL, 2.35 mmol) was added. 4,4'-Dicarboxysuccinimidyl-2,2'-bipyridine (438 mg, 1 mmol) in dry DMF was added dropwise into the solution and stirred for 24 h at room temperature (RT). After the solvent was removed under reduced pressure, the reaction mixture was subjected to HPLC purification to yield pure compound **1** (740 mg, 78%) (Scheme S1, Supporting Information). Mass of **1**: calculated for $C_{54}H_{53}N_6O_{10}$, $[(M+H)^+]$: 945.3823, obsvd. HR-MALDI-TOF/MS: 945.3824 (Fig. S2†). ^{1}H NMR of **1** (300 MHz, d_6-DMSO, Fig. S3†) δ (ppm): 8.97 (s, 2 H), 8.84 (d, J = 6.0 Hz, 2 H), 8.80 (s, 2 H), 7.81-7.92 (m, 6 H), 7.62-7.75 (m, 6 H), 7.40 (t, J = 6.0 Hz, 4 H), 7.30 (t, J = 6.0 Hz, 4 H), 4.16-4.33 (m, 6 H), 3.96 (m, 6 H), 3.27-3.37 (m, 4 H), 1.3-1.85 (m, 12 H); ^{13}C NMR of **1** (75 MHz, d_6-DMSO, Fig. S4†) δ (ppm): 173.99, 164.40, 156.16, 155.35, 149.87, 143.76, 143.01, 140.66, 127.58, 125.22, 121.93, 120.05, 118.24, 65.55, 53.73, 46.61, 30.43, 28.47, 23.15.

Cell culture

The hepatocellular carcinoma HepG2 cells were cultured in Dulbecco's modified eagle medium (DMEM, GIBCO) supplemented with 10% fetal bovine serum (FBS, GIBCO) and streptomycin (100 µg/mL). The cells were expanded in tissue culture dishes and kept in a humidified atmosphere of 5% CO_2 at 37 °C. The medium was changed every other day.

MTT Assay

The cytotoxicity was measured using the 3-(4, 5-dimethylthiazol-2-yl)-2, 5-diphenyltetrazolium bromide (MTT) assay with HepG2 or LoVo cells. Cells growing in log phase were seeded into 96-well cell-culture plate at 3×10^3/well. The cells were incubated for 12 h at 37 °C under 5% CO_2. The solutions of **1** (100 µL/well) at concentrations of 20, 40 or 80 µM in 100 µL medium were added to the wells, respectively. The cells were incubated for 1, 2 and 3 day at 37 °C under 5% CO_2. A solution of 5 mg/mL MTT dissolved in phosphate buffered saline (PBS) (pH 7.4) (10 µL /well) was added to each well of the 96-well plate. A solution of 10% SDS dissolved in 0.01M HCl (100 µL/well) was added to dissolve the formazan after an additional 4 h-incubation. The data were obtained using an ELISA reader (VARIOSKAN FLASH) to detect its absorption at 570/680 nm. The following formula was used to calculate the viability of cell growth: Viability (%) = (mean of Absorbance value of treatment group / mean of Absorbance value of control) ×100.

Cell imaging

The hepatocellular carcinoma HepG2 cells were plated on 3.5 cm cell culture dish at 50% cell density the next day. Then the HepG2 or LoVo cells were washed three times with phosphate buffered saline (PBS) and incubated with 0, 5, 10, or 20 µM Cd^{2+} in serum-free medium at 37 °C for 0.5 h in a CO_2 incubator. The cells were then washed with PBS and incubated with 20 µM **1** in serum-free medium for 0.5 h at 37 °C. Then, the cells were washed with PBS another three times prior to microscopic imaging.

PH-controlled gelation of 1

7 mg of **1** was suspended in 400 µL water. Adjustment of the pH value of above suspension to 8.5 with 1 M NaOH solution resulted in clear solution. Carefully adjusting the pH value of above solution to 5.5 with 0.1 M HCl afforded opaque **Gel I** (the inset in Fig. 5a). For Cd^{2+}-containing **Gel I**, Cd^{2+} solution (1.48 M, 5 µL, 1 equiv. to **1**) was added into the turbid suspension of **1** (16.5 mM) at pH 6. Then

the pH value of the mixture was adjusted to 5.5 to afford opaque Cd^{2+}-containing **Gel I**. (the inset in Fig. 5c).

Theoretical simulations

Molecular models for all the compounds were built with the Gauss View package. Geometry optimization and electronic structure have been carried out at the hybrid density function theory (DFT) B3LYP level using the Gaussian09 program.[47] The solvent effect was considered with the polarizable continuum model (PCM). Time-dependent DFT (TDDFT) calculations at the same level[48] were carried out to find out the excited states, with which we predicted the absorbance spectra and fluorescence behavior.

Acknowledgements

This work was supported by Collaborative Innovation Center of Suzhou Nano Science and Technology, the Major Program of Development Foundation of Hefei Center for Physical Science and Technology, and the National Natural Science Foundation of China (Grants 21175122, 91127036, and 21375121).

Notes and references

[a]CAS Key Laboratory of Soft Matter Chemistry, Department of Chemistry, University of Science and Technology of China, Hefei, Anhui 230026, China
[b]Key Laboratory of Separation Sciences for Analytical Chemistry, Dalian Institute of Chemical Physics, Chinese Academy of Sciences, Dalian 116023, China
[c]Department of Chemical Physics, University of Science and Technology of China, 96 Jinzhai Road, Hefei, Anhui 230026, China.
[d]Center for Integrative Imaging, Hefei National Laboratory for Physical Sciences at the Microscale & School of Life Sciences, University of Science and Technology of China, Hefei, Anhui 230026, China
E-mail: jiangj1@ustc.edu.cn (J.J.), gliang@ustc.edu.cn (G.-L. L.).
Electronic Supplementary Information (ESI) available: Synthetic routes; Supporting Figs. S1-17 and Tables S1-3. See DOI: 10.1039/b000000x/

1 X. J. Peng, J. J. Du, J. L. Fan, J. Y. Wang, Y. K. Wu, J. Z. Zhao, S. G. Sun and T. Xu, *J. Am. Chem. Soc.*, 2007, **129**, 1500-1501.
2 C. N. McFarland, L. I. Bendell-Young, C. Guglielmo and T. D. Williams, *J. Environ. Monit.*, 2002, **4**, 791-795.
3 A. N. Anthemidis and C. P. P. Karapatouchas, *Microchim. Acta* 2008, **160**, 455-460.
4 G. Kaya and M. Yaman, *Talanta*, 2008, **75**, 1127-1133.
5 D. Colbert, K. S. Johnson and K. H. Coale, *Anal. Chim. Acta* 1998, **377**, 255-262.
6 X. W. Guo and X. M. Guo, *Anal. Chim. Acta*, 1995, **310**, 377-385.
7 A. Montaser and V. A. Fassel, *Anal. Chem.*, 1976, **48**, 1490-1499.
8 T. Balaji, M. Sasidharan and H. Matsunaga, *Anal. Bioanal. Chem.*, 2006, **384**, 488-494.
9 Y. Xue, H. Zhao, Z. J. Wu, X. J. Li, Y. J. He and Z. B. Yuan, *Analyst*, 2011, **136**, 3725-3730.
10 A. C. Davis, C. P. Calloway and B. T. Jones, *Talanta*, 2007, **71**, 1144-1149.
11 S. N. Willie, Y. Iida and J. W. McLaren, *Atom. Spectrosc.*, 1998, **19**, 67-72.
12 L. Ahlgren and S. Mattsson, *Phys. Med. Biol.*, 1981, **26**, 19-26.
13 A. M. Bond and G. G. Wallace, *Anal. Chem.*, 1984, **56**, 2085-2090.
14 J. Yin, T. Wu, J. B. Song, Q. Zhang, S. Y. Liu, R. Xu and H. W. Duan, *Chem. Mater.*, 2011, **23**, 4756-4764.
15 T. Y. Cheng, Y. F. Xu, S. Y. Zhang, W. P. Zhu, X. H. Qian and L. P. Duan, *J. Am. Chem. Soc.*, 2008, **130**, 16160-16161.
16 A. M. Tang, B. Mei, W. J. Wang, W. L. Hu, F. Li, J. Zhou, Q. Yang, H. Cui, M. Wu and G. L. Liang, *Nanoscale*, 2013, **5**, 8963-8967.
17 R. Huang, X. J. Wang, D. L. Wang, F. Liu, B. Mei, A. M. Tang, J. Jiang and G. L. Liang, *Anal. Chem.*, 2013, **85**, 6203-6207.
18 L. Xue, C. Liu and H. Jiang, *Org. Lett.*, 2009, **11**, 1655-1658.
19 S. Y. Park, J. H. Yoon, C. S. Hong, R. Souane, J. S. Kim, S. E. Matthews and J. Vicens, *J. Org. Chem.*, 2008, **73**, 8212-8218.
20 A. Varriale, M. Staiano, M. Rossi and S. D'Auria, *Anal. Chem.*, 2007, **79**, 5760-5762.
21 S. Banerjee, S. Kara and S. Santra, *Chem. Commun.*, 2008, 3037-3039.
22 G. J. Tian and Y. Luo, *Angew. Chem. Int. Ed.*, 2013, **52**, 4814-4817.
23 Y. Y. Zhao and X. Y. Jiang, *Nanoscale*, 2013, **5**, 8340-8350.
24 Y. L. Xianyu, J. S. Sun, Y. X. Li, Y. Tian, Z. Wang and X. Y. Jiang, *Nanoscale*, 2013, **5**, 6303-6306.
25 Y. M. Yang, F. Liu, X. G. Liu and B. G. Xing, *Nanoscale*, 2013, **5**, 231-238.
26 S. Charles, S. Yunus, F. Dubois and E. Vander Donckt, *Anal. Chim. Acta*, 2001, **440**, 37-43.
27 Z. Wang, M. A. Palacios and P. Anzenbacher, *Anal. Chem.*, 2008, **80**, 7451-7459.
28 M. C. Aragoni, M. Arca, F. Demartin, F. A. Devillanova, F. Isaia, A. Garau, V. Lippolis, F. Jalali, U. Papke, M. Shamsipur, L. Tei, A. Yari and G. Verani, *Inorg. Chem.*, 2002, **41**, 6623-6632.
29 X. Jiang, B. G. Park, J. A. Riddle, B. J. Zhang, M. Pink and D. Lee, *Chem. Commun.*, 2008, 6028-6030.
30 J. Wei, H. M. Wang, M. F. Zhu, D. Ding, D. X. Li, Z. N. Yin, L. Y. Wang and Z. M. Yang, *Nanoscale*, 2013, **5**, 9902-9907.
31 W. J. Wang, J. C. Qian, A. M. Tang, L. N. An, K. Zhong and G. L. Liang, *Anal. Chem.*, 2014, **86**, 5955-5961.
32 Y. Kuang, Y. Gao, J. F. Shi, J. Li and B. Xu, *Chem. Commun.*, 2014, **50**, 2772-2774.
33 A. M. Tang, W. J. Wang, B. Mei, W. L. Hu, M. Wu and G. L. Liang, *Sci. Rep.*, 2013, **3**, 1848.
34 Y. Zhang, B. Zhang, Y. Kuang, Y. Gao, J. F. Shi, X. X. Zhang and B. Xu, *J. Am. Chem. Soc.*, 2013, **135**, 5008-5011.
35 T. Su, Z. Tang, H. J. He, W. J. Li, X. Wang, C. N. Liao, Y. Sun and Q. G. Wang, *Chem. Sci.*, 2014, **5**, 4204-4209.
36 X. H. Liu, D. B. Wu, H. L. Wang and Q. G. Wang, *Adv. Mater.*, 2014, **26**, 4370-4375.
37 V. Jayawarna, M. Ali, T. A. Jowitt, A. E. Miller, A. Saiani, J. E. Gough and R. V. Ulijn, *Adv. Mater.*, 2006, **18**, 611-614.
38 M. Ikeda, T. Tanida, T. Yoshii, K. Kurotani, S. Onogi, K. Urayama and I. Hamachi, *Nat. Chem.*, 2014, **6**, 511-518.
39 Y. B. Cai, Y. Shi, H. M. Wang, J. Y. Wang, D. Ding, L. Wang and Z. M. Yang, *Anal. Chem.*, 2014, **86**, 2193-2199.
40 K. M. Xu, W. W. Ge, G. L. Liang, L. Wang, Z. M. Yang, Q. G. Wang, I. M. Hsing and B. Xu, *Int. J. Radiat. Biol.*, 2008, **84**, 353-362.
41 Z. M. Yang, K. M. Xu, L. Wang, H. W. Gu, H. Wei, M. J. Zhang and B. Xu, *Chem. Commun.*, 2005, 4414-4416.

42 K. F. Lam, K. L. Yeung and G. Mckay, *Environ. Sci. Technol.*, 2007, **41**, 3329-3334.
43 G. M. Cockrell, G. Zhang, D. G. VanDerveer, R. P. Thummel and R. D. Hancock, *J. Am. Chem. Soc.*, 2008, **130**, 1420-1430.
44 F. Grimm, K. Hartnagel, F. Wessendorf and A. Hirsch, *Chem. Commun.*, 2009, 1331-1333.
45 X. L. Tang, X. H. Peng, W. Dou, J. Mao, J. R. Zheng, W. W. Qin, W. S. Liu, J. Chang and X. J. Yao, *Org. Lett.*, 2008, **10**, 3653-3656.
46 X. Z. Yan, S. J. Li, T. R. Cook, X. F. Ji, Y. Yao, J. B. Pollock, Y. H. Shi, G. C. Yu, J. Y. Li, F. H. Huang and P. J. Stang, *J. Am. Chem. Soc.*, 2013, **135**, 14036-14039.
47 M. J. Frisch, G. W. Trucks, H. B. Schlegel, G. E. Scuseria, M. A. Robb, J. R. Cheeseman, G. Scalmani, V. Barone, B. Mennucci and G. A. Petersson, *Gaussian Inc. Revision A.1.*, **2009**.
48 M. Caricato, B. Mennucci, J. Tomasi, F. Ingrosso, R. Cammi, S. Corni and G. Scalmani, *J. Chem. Phys.*, 2006, **124**, 124520.